核子类时电磁形状因子振荡的模型解释

刘占伟

兰州大学物理科学与技术学院

Ri-Qing Qian, Zhan-Wei Liu, Xu Cao, Xiang Liu,
A toy model to understand oscillatory behavior in time-like nucleon form factors,
Accepted as a letter in Phys. Rev. D

CONTENTS

Introduction to the electromagnetic form factors

Electromagnetic form factors

- Electromagnetic form factors can help disclose the hadron structures and complicated interactions

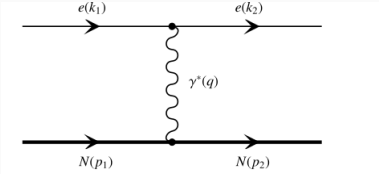

One-photon exchange diagram for elastic scattering, $e + N \to e + N$

for nucleon,

$$\langle N|J^\mu|N\rangle = \bar{u}(p_2)\,[F_1(q^2)\gamma^\mu - F_2(q^2)\frac{\sigma^{\mu\nu}q_\nu}{2M}]\,u(p_1)$$

for $\Delta(1232)$,

$$\langle T(p')|J_\mu|T(p)\rangle = \bar{u}^\rho(p')O_{\rho\mu\sigma}(p',p)u^\sigma(p),$$

$$O_{\rho\mu\sigma}(p',p) = g_{\rho\sigma}(A_1\gamma_\mu + \frac{A_2}{2M_T}P_\mu) + \frac{q_\rho q_\sigma}{(2M_T)^2}(C_1\gamma_\mu + \frac{C_2}{2M_T}P_\mu).$$

- Usually for a particle with spin J, it has $2J+1$ electromagnetic form factors.
- From these form factors, we can extract the magnetic moments, electromagnetic radius, and so on.

Electromagnetic form factors

- Electromagnetic form factors can help disclose the hadron structures and complicated interactions

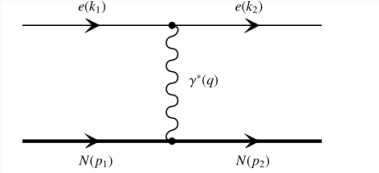

One-photon exchange diagram for elastic scattering, $e + N \to e + N$

for nucleon,

$$\langle N|J^\mu|N\rangle = \bar{u}(p_2)\,[F_1(q^2)\gamma^\mu - F_2(q^2)\frac{\sigma^{\mu\nu}q_\nu}{2M}]\,u(p_1)$$

for $\Delta(1232)$,

$$\langle T(p')|J_\mu|T(p)\rangle = \bar{u}^\rho(p')O_{\rho\mu\sigma}(p',p)u^\sigma(p),$$

$$O_{\rho\mu\sigma}(p',p) = g_{\rho\sigma}(A_1\gamma_\mu + \frac{A_2}{2M_T}P_\mu) + \frac{q_\rho q_\sigma}{(2M_T)^2}(C_1\gamma_\mu + \frac{C_2}{2M_T}P_\mu).$$

- Usually for a particle with spin J, it has $2J+1$ electromagnetic form factors.
- From these form factors, we can extract the magnetic moments, electromagnetic radius, and so on.
- In our previous woks (PhysRevD.95.076001, ...), we showed the chiral loop correction is important for the space-like electromagnetic form factors.

Pion Photoproduction off Nucleon with Hamiltonian EFT

- combining
  - $\pi N \to \pi N$
  - lattice QCD data
  - $\gamma + N \to \pi + N$
- $\gamma + N \to \pi + N$
  - γNN etc. couplings are not adjusted

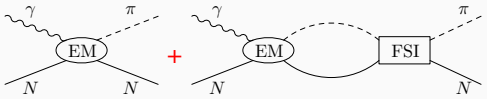

$$\mathcal{M}(\gamma N \to \pi N) \sim \mathcal{M}^{\mathrm{EM}}(\gamma N \to \pi N) + \mathcal{M}^{\mathrm{EM}}(\gamma N \to \pi N) \otimes \mathcal{M}^{\mathrm{FSI}}(\pi N \to \pi N) + \mathcal{M}^{\mathrm{EM}}(\gamma N \to \eta N) \otimes \mathcal{M}^{\mathrm{FSI}}(\eta N \to \pi N)$$

  - understand the structure of $N(1535)$ and the interactions of $\pi N / \eta N$ at low energies and near the resonance
  - necessities for the photon-nucleus investigation

Z. W. Liu, W. Kamleh, D. B. Leinweber, F. M. Stokes, A. W. Thomas and J. J. Wu, Phys. Rev. Lett. 116 (2016) no.8, 082004

D. Guo and Z. W. Liu, Phys. Rev. D **105** (2022) no.11, 11

time-like form factors

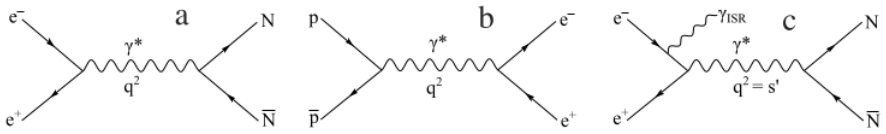

Fig. 1. Diagrammatic representation of the experimental processes used for the measurement of timelike nucleon FF's: (a) e^+e^- ann experiments; (b) $p\bar{p}$ annihilation; (c) the initial state radiation technique at e^+e^- colliders; in all cases the form factor is measured as a f square four-momentum transfer and q^2 of the virtual photon coupling to the baryon pair.

For these processes, it also related to $F_1(q^2)$ and $F_2(q^2)$ but with $q^2 > 0$ while $q^2 < 0$ for eN scattering process.

Time-like and space-like form factors are analytically connected.

Damped oscillation of nucleon electromagnetic form factors

Observation of oscillation in time-like electromagnetic form factors

- Bianconi and Tomasi-Gustafsson first pointed out an unexpected oscillation behavior in the near-threshold region.

- The effective form factors G_{eff} of the nucleons were found to be well divided into two parts.
  - The main part G^0 can be obtained with a perturbative QCD parametrization and describes the main decreasing behavior of the form factor very well
  - the remaining part G^{osc} exhibits a damped oscillation with regularly spaced maxima and minima over the sub-GeV scale.

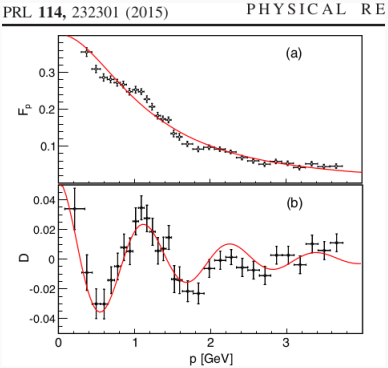

Extensions to other baryon-antibaryon production

$e^+e^- \to \Lambda\bar{\Lambda}, \Sigma^0\bar{\Sigma}^0, \Xi^0\bar{\Xi}^0, \ldots$ were also studied. The oscillating behavior need to be confirmed by future precise experiments.

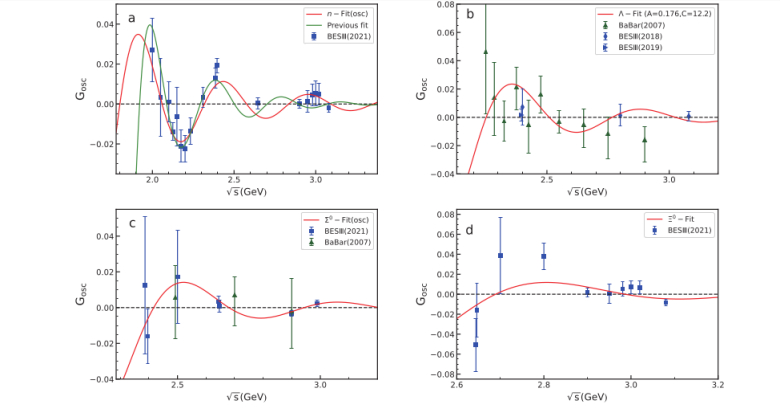

Fig. 3. (color online) Fitting results of the oscillating component of the neutron (a), Λ (b), Σ^0 (c), and Ξ^0 (d) effective form factors.

An-Xin Dai, Zhong-Yi Li, Lei Chang, Ju-Jun Xie, Chin. Phys. C 46, 073104 (2022)

Possible mechanisms

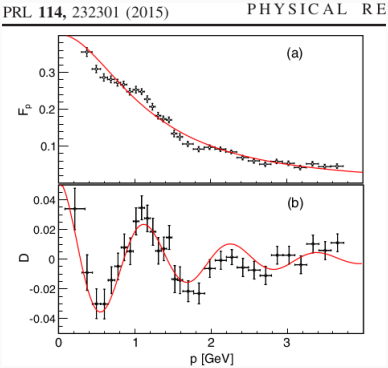

Possible mechanisms

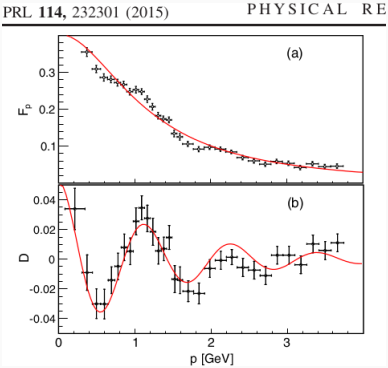

- vector meson dominance

Possible mechanisms

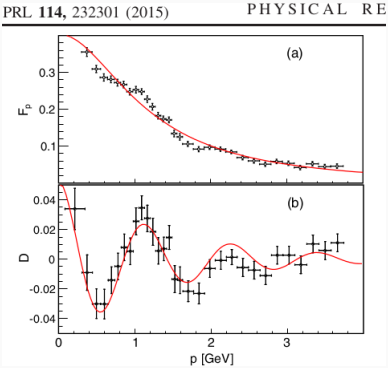

- vector meson dominance
- cusp effects from coupled channels (baryon-antibaryon channels)

Possible mechanisms

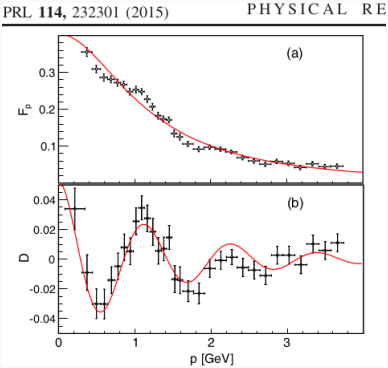

- vector meson dominance
- cusp effects from coupled channels (baryon-antibaryon channels)
- finite-state interaction

Possible mechanisms

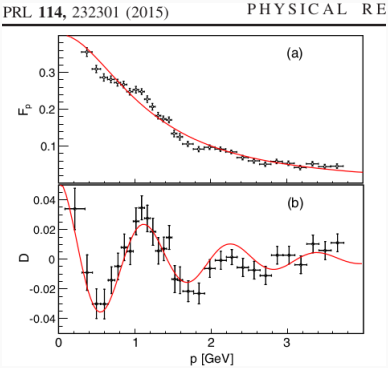

- vector meson dominance
- cusp effects from coupled channels (baryon-antibaryon channels)
- finite-state interaction
- …

Vector-meson dominance

S. Pacetti et al. / Physics Reports 550–551 (2015) 1–103

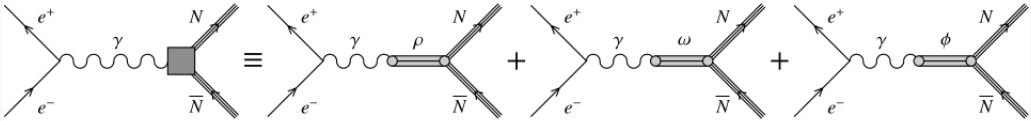

Fig. 15. Feynman diagram of the nucleon FFs in terms of the VMD_I contributions of the isovector meson ρ and the isoscalar mesons ω and ϕ.

Vector-meson dominance with the nucleon Bethe-Salpeter amplitude

A 2009 study, based on suitable ansatzes for the nucleon Bethe-Salpeter amplitude and a microscopic version of the well-known Vector Meson Dominance mode, showed oscillatory structures.

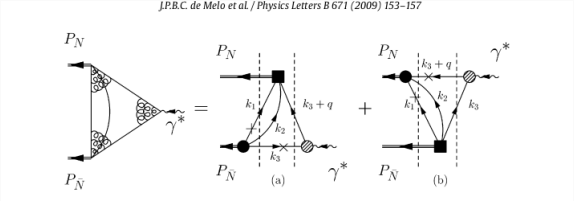

Fig. 2. Diagrams contributing to the TL nucleon FF: (a) $P_N^+ < k_3^+ + q^+ < q^+$; (b) $0 \leqslant k_3^+ + q^+ \leqslant P_N^+$. Symbols as in Fig. 1.

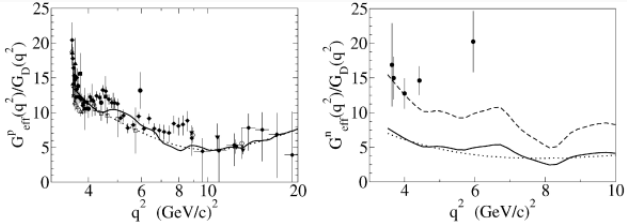

Interference between the dipole and oscillation terms

From

$$G_N = G_N^D + \frac{I_N^{\rm rsd}}{\sqrt{2}} \qquad \&$$

$$|G_N| = G_N^D + G_N^{\rm rsd},$$

one can easily get

$$G_N^{\rm rsd} = \frac{|I_N^{\rm rsd}|}{\sqrt{2}} \cos(\phi_N^D - \phi_N^{\rm rsd}) + o(\frac{I_N^{\rm rsd}}{G_N^D})$$

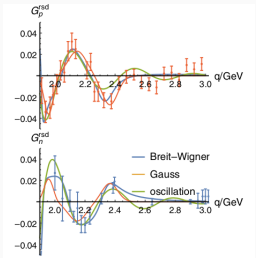

FIG. 1. The fit of the Breit-Wigner distribution and the Gauss distribution to three local structures below 2.5 GeV in comparison with BESIII data [16,18].

XU CAO, JIAN-PING DAI, and HORST LENSKE PHYS. REV. D **105,** L071503 (2022)

TABLE I. Parameters of three local structures below 2.5 GeV in the fit of the Breit-Wigner distribution (or Gauss distribution in the parentheses), together with the extracted $\Gamma_{ee}\Gamma_{N\bar{N}}$ for the Breit-Wigner distribution. The χ^2/d.o.f is 0.7 (1.2).

k/BW(GS)	1	2	3
M_k (MeV)	1910 ± 10 (1958 ± 10)	2083 ± 27 (2148 ± 16)	2328 ± 22 (2365 ± 13)
Γ_k (MeV)	32 ± 32 (30 ± 8)	162 ± 55 (60 ± 17)	162 ± 57 (52 ± 14)
δ^k	-0.072 ± 0.048 (-0.036 ± 0.010)	0.041 ± 0.007 (0.024 ± 0.005)	-0.032 ± 0.005 (-0.027 ± 0.007)
$\phi_p^D - \phi^k$	0	0.764 ± 0.373 (0.235 ± 0.307)	1.558 ± 0.310 (0.046 ± 0.241)
$\Gamma_{ee}\Gamma_{N\bar{N}}$ (keV^2)	4 ± 4	80 ± 47	62 ± 37

Dispersion relations

Applying Cauchy's theorem to $F(t)$, one gets

$$F(t) = \lim_{\epsilon \to 0^+} \frac{1}{\pi} \int_{t_0}^{\infty} \frac{\mathrm{Im}\, F(t')}{t' - t - i\epsilon} dt'$$

and other dispersion relations.

$\mathrm{Im}\, F(t)$ comes from 2π, 3π, $K\bar{K}$, 10+ explicitly resonances, and so on.

Some resonances like ρ are naturally dynamically generated, while others like ϕ are not.

TABLE I. Datasets included in the combined space- and timelike fits. See Ref. [40] and the Supplemental Material [15] for explicit references.

Data type	Range of $\lvert t\rvert$ (GeV^2)	Number of data
$\sigma(E,\theta)$, PRad	0.000 215–0.058	71
$\sigma(E,\theta)$, MAMI	0.003 84–0.977	1422
$\mu_p G_E^p/G_M^p$, JLab	1.18–8.49	16
G_E^n, world	0.14–1.47	25
G_M^n, world	0.071–10.0	23
$\lvert G_{\mathrm{eff}}^p\rvert$, world	3.52–20.25	153
$\lvert G_{\mathrm{eff}}^n\rvert$, world	3.53–9.49	27
$\lvert G_E/G_M\rvert$, *BABAR*	3.52–9.0	6
$d\sigma/d\Omega$, BESIII	1.88^2–1.95^2	10

$$|G_{\mathrm{eff}}| \equiv \sqrt{\frac{|G_E|^2 + \xi |G_M|^2}{1+\xi}}, \qquad (4)$$

with $\xi = t/(2m^2)$. However, there are also some data for the ratio $|G_E/G_M|$ and some differential cross section data from *BABAR* and BESIII. The phase of the ratio G_E/G_M has not been measured. It turns out that a certain number of broad poles above threshold is needed to get a good

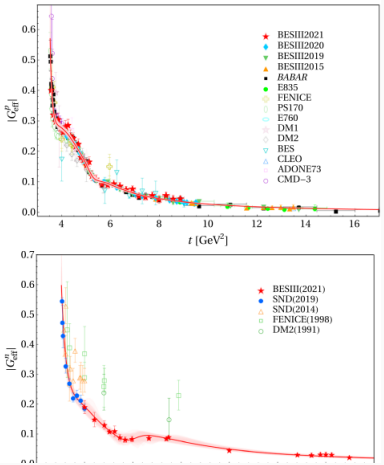

Yong-Hui Lin, Hans-Werner Hammer, Ulf-G. Meißner

Cusp effect from coupled channels

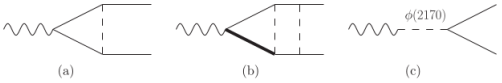

$$C_0(\kappa = p_k, p_l, m_1, m_2, m_3) = \frac{1}{i\pi^2} \int \frac{d^4k}{[k^2 - m_1^2][(k - p_k)^2 - m_2^2][(k + p_l)^2 - m_3^2]} \quad (12)$$

FIG. 1. The different types of diagrams contributing to the NFFs above the $p\bar{p}$ threshold, as discussed in Sec. I B. Th
denotes the photon, the thin solid line the (anti)nucleon, the thick solid line an (anti)nucleon resonance and the dashed line denotes all
possible mesons, e.g. pions in (a)+(b) and the vector meson $\phi(2170)$ in (c).

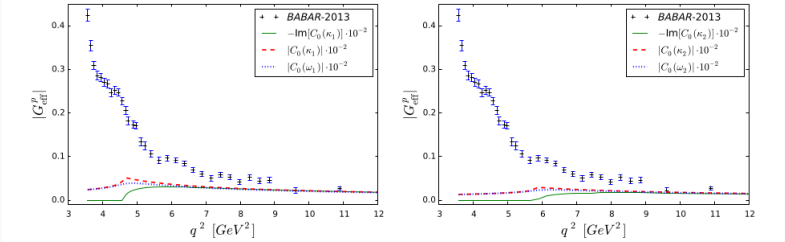

FIG. 11 (color online). The q^2-dependence from the scalar Passarino-Veltman triangle diagrams with virtual $N\bar{\Delta}\pi$ and $\Delta\bar{\Delta}\pi$ states compared to G^p_{eff} from Ref. [24].

The inclusion of the Δ width partly smears out the cusp effect.

Final-state interaction mechanism

Distorted wave Born approximation:

$$f_L^{\bar{N}N}(k;E_k) \;=\; f_L^{\bar{N}N,0}(k) + \sum_{L'}\int_0^\infty \frac{dpp^2}{(2\pi)^3} f_{L'}^{\bar{N}N,0}(p)\frac{1}{2E_k - 2E_p + i0^+} T_{L'L}(p,k;E_k),$$

where (f^0) f is the (bare) $\gamma N\bar{N}$, and T is the $N\bar{N}$ scattering amplitude.

For threshold enhancement of cross section

$$G_{\rm osc}^N(\tilde{p}) = G_{{\rm osc},1}^{0,N}(0)\tilde{E}_{\alpha_1^N,1}(-\omega_1^2\tilde{p}^{\alpha_1^N}) + G_{{\rm osc},2}^{0,N}(0)\tilde{E}_{\alpha_2^N,1}(-\omega_2^2(\tilde{p}+p_0^N)^{\alpha_2^N}), \qquad (7)$$

with the Mittag-Leffler function $\tilde{E}_{\alpha,\beta}(z)$ given by [50]

$$\tilde{E}_{\alpha,\beta}(z) = \sum_{k=0}^{\infty}\frac{z^k}{\Gamma(\alpha k+\beta)}. \qquad (8)$$

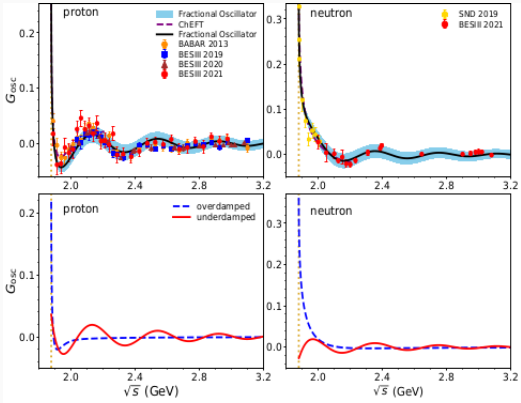

FIG. 2. Results for the SFFs $G_{\rm osc}^N(\tilde{p})$ with fractional oscillation functions. See Eqs. (6,7). The yellow dotted lines are the thresholds. The uncertainty bands are estimated from bootstrap [51], within 1 σ. The individual contributions of the 'overdamped' and 'underdamped' oscillators to $G_{\rm osc}$ are shown at the bottom.

Qin-He Yang, Ling-Yun Dai, Di Guo, Johann Haidenbauer, Xian-Wei Kang, Ulf-G. Meißner, arXiv: 2206.01494

A toy model to understand oscillatory behavior in time-like nucleon form factors

Separation of formation and rescattering process

- short-range formation process
  - production of $N\bar{N}$
  - $N\bar{N}$ scattering due to annihilation and short-range interaction

  they are strongly tangled since the interaction ranges are similar, $\sim 1/2m_N$.

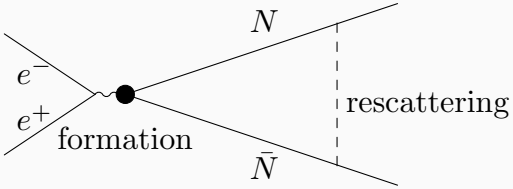

- long-range rescattering process
  the interaction range is $\sim 1/m_\pi$

$$\frac{1/(2m_N)}{1/m_\pi} \approx 14$$

Distorted-wave Born approximation

With classical distorted-wave Born approximation,

$$\sigma = \frac{1}{|\mathcal{J}(p)|^2}\sigma_0\,.$$

where Jost function is

$$\mathcal{J}(p) \approx \mathcal{J}_{\ell=0}(p) = \lim_{r\to 0}\frac{j_0(pr)}{\psi_{0,p}(r)}\,.$$

The regular spherical Bessel function $j_0(pr) = \sin(pr)$ is the free radial solution of Schrödinger equation.

With the proper $N\bar{N}$ potential V

$$\left(\frac{d^2}{dr^2} - \frac{\ell(\ell+1)}{r^2} - 2\mu V + p^2\right)\psi_{\ell,p}(r) = 0\,,$$

Reproduction of Sommerfeld factor within our scheme

Sommerfeld factor has been widely used in extracting the form factors of nucleons from the cross sections

$$|G_{\text{eff}}(s)| = \sqrt{\frac{3s}{4\pi\alpha^2\beta C(1+2m_N^2/s)}\,\sigma_{e^+e^-\to N\bar{N}}}\,.$$

- it arises from the long-range Coulomb interaction
- for $e^+e^- \to p\bar{p}$ cross sections

$$C = |\frac{1}{\mathcal{S}^2}|, \quad \mathcal{S} = \left(\frac{y}{1-e^{-y}}\right)^{-1/2}, \quad y = \frac{\pi\alpha\sqrt{1-\beta^2}}{\beta}.$$

- for $e^+e^- \to n\bar{n}$, $C = 1$, no such correction.

Reproduction of Sommerfeld factor within our scheme

Sommerfeld factor has been widely used in extracting the form factors of nucleons from the cross sections

$$|G_{\text{eff}}(s)| = \sqrt{\frac{3s}{4\pi\alpha^2\beta C(1+2m_N^2/s)}\,\sigma_{e^+e^-\to N\bar{N}}}\,.$$

- it arises from the long-range Coulomb interaction
- for $e^+e^- \to p\bar{p}$ cross sections

$$C = |\frac{1}{\mathcal{S}^2}|, \quad \mathcal{S} = \left(\frac{y}{1-e^{-y}}\right)^{-1/2}, \quad y = \frac{\pi\alpha\sqrt{1-\beta^2}}{\beta}.$$

- for $e^+e^- \to n\bar{n}$, $C = 1$, no such correction.

We can easily reproduce this famous Sommerfeld factor

- with the formalism on the previous page
- substituting V with the Coulomb potential
- using the non-relativistic approximation $\sqrt{1-\beta^2} \approx 1$ in the near-threshold region

A toy model

If the $N\bar{N}$ potential is as follows,

$$V(r) = \begin{cases} -V_a & \text{for} \quad 0 \leqslant r < a \\ 0 & \text{for} \quad r \geqslant a \end{cases} .$$

we have

$$\psi_{0,p}(r) = \begin{cases} \dfrac{e^{i\delta_0}\sin(p_{in}r)}{\sqrt{\sin^2(p_{in}a) + \frac{p^2}{p_{in}^2}\cos^2(p_{in}a)}} & \text{for} \quad 0 \leqslant r < a \\ e^{i\delta_0}\sin(pr + \delta_0) & \text{for} \quad r \geqslant a \end{cases} ,$$

where δ_0 is the S-wave phase shift, and

$$p_{in} = \sqrt{p^2 + 2\mu V_a}.$$

We have the enhancement factor $|1/\mathcal{J}|^2 > 1$ for the pure attractive interaction

$$|\mathcal{J}(p)| = \sqrt{\frac{p^2}{p_{in}^2}\sin^2(p_{in}a) + \cos^2(p_{in}a)}\,.$$

The enhancement factor with the toy model

$$|G_{\text{eff}}(s)| = \frac{1}{|\mathcal{J}|}\, G_0(s)\,, \qquad |\mathcal{J}(p)| = \sqrt{\frac{p^2}{p_{in}^2}\sin^2(p_{in}a) + \cos^2(p_{in}a)}\,.$$

- The energy gaps between the 1st, the 2nd, the 3rd and the 4th minima are:

$$\frac{3\pi^2}{2\mu a^2}, \quad \frac{5\pi^2}{2\mu a^2}, \quad \frac{7\pi^2}{2\mu a^2}\,.$$

- $\mu = m_N/2$ and $a \approx 1/m_\pi$ give the 1st gap $\Delta E_1 \approx 0.6$ GeV.
  This is close to the value observed in experiment.

- The peaks $|1/\mathcal{J}|^2_{\max} = 1 + 2\mu V_a/p^2$ decrease with the increasing energies.

Different potentials and enhancement factors

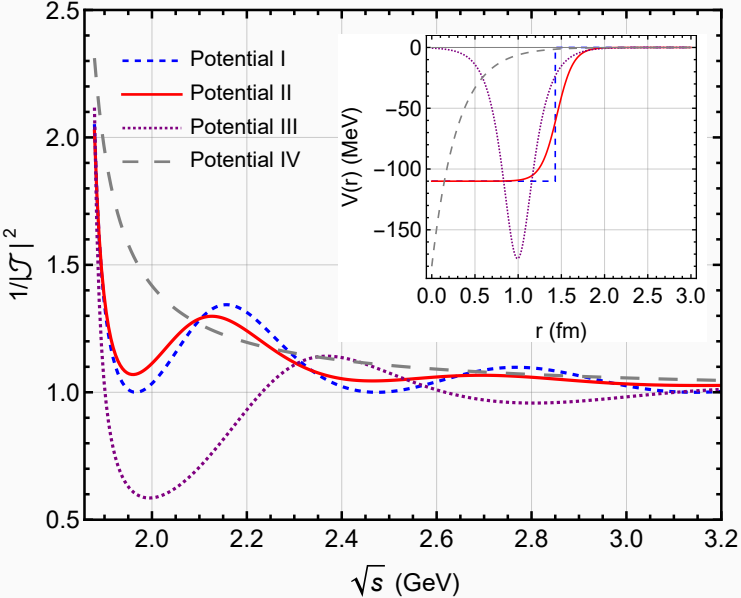

Description for the effective form factors

To fit the main part, we use the following expression from Ref. [BESIII:2019hdp]

$$G_0(s) = \frac{\mathcal{A}}{(1 + s/m_a^2)\,[1 - s/(0.71\ \mathrm{GeV}^2)]^2}\,,$$

where $m_a^2 = 7.72\ \mathrm{GeV}^2$ and $\mathcal{A}$ is a constant. With fitted $\mathcal{A}_p = 9.37$ and $\mathcal{A}_n = 5.8$.

For the oscillatory part,

$$G^{osc}(s) = |G_{\mathrm{eff}}| - G_0 = \left(\frac{1}{|\mathcal{J}|} - 1\right) G_0(s)\,.$$

we use the following potential to get the $\mathcal{J}$

$$V(r) = \begin{cases} -V_r & 0 \leqslant r < a_r \\ -V_a & a_r \leqslant r < a \\ 0 & r \geqslant a \end{cases},$$

where $0 < V_r < V_a$ and
we take $a_r = 0.5$ fm.

Table 1: Parameters for $p\bar{p}$ and $n\bar{n}$ potential.

$N\bar{N}$	a_r (fm)	V_r (MeV)	a (fm)	V_a (MeV)
$p\bar{p}$	0.5	50	1.6	90
$n\bar{n}$	0.5	400	1.4	650

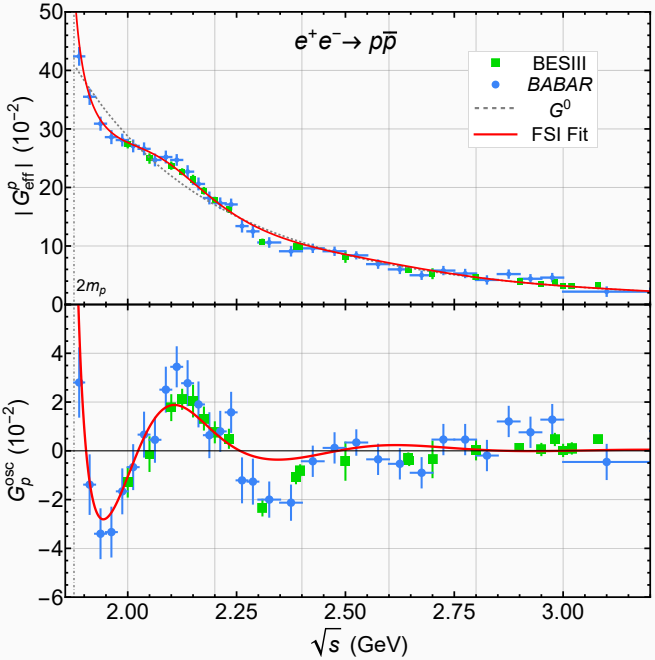
$e^+e^- \to p\bar{p}$
BESIII
BABAR
G^0
FSI Fit
$|G_{\rm eff}^p|$ (10^{-2})
$2m_p$
$G_p^{\rm osc}$ (10^{-2})
$\sqrt{s}$ (GeV)

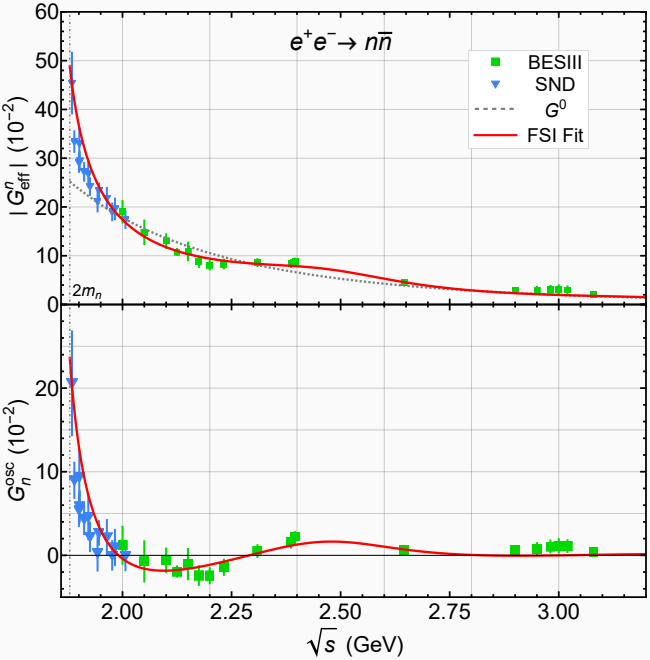
$e^+e^- \to n\bar{n}$
BESIII
SND
G^0
FSI Fit
$|G_{\rm eff}^n|$ (10^{-2})
$2m_n$
$G_n^{\rm osc}$ (10^{-2})
$\sqrt{s}$ (GeV)

Short discussion of numerical results

- The overall oscillatory behavior is well reproduced by the FSI effect with the interaction range a about $1.4 \sim 1.6$ fm.

- The details of the description of the effective form factors depend on the choice of the continuum part G_0, which we still do not understand very well, because the formation process involves the complicated hadronization and other difficulties.

- Perhaps better descriptions can be obtained for $|G_{\mathrm{eff}}|$ by using different G_0 rather than the same as in the experimental collaborations.

Threshold enhancement on cross sections for baryon-antibaryon productions

- The SND measurement observed the enhancement on the neutron cross section just above threshold at $\sqrt{s} - 2m_n \approx 5$ MeV, which contradicts the naive phase space expectation.

  (Ref. [SND:2022wdb])

- Abnormally large cross sections are observed in $e^+e^- \to \Lambda\bar{\Lambda}$ near the threshold $\left(\sqrt{s} - 2m_\Lambda\right) \approx 1$ MeV and possibly $e^+e^- \to \Lambda_c\bar{\Lambda}_c$ at $\left(\sqrt{s} - 2m_{\Lambda_c}\right) \approx 1.58$ MeV.

  (Refs.[BESIII:2017hyw,BESIII:2017kqg])

- However, no such phenomenon were found in the $\Xi\bar{\Xi}$ and $\Sigma\bar{\Sigma}$ productions.

  (Refs.[BESIII:2020ktn,BESIII:2021aer,BESIII:2020uqk,BESIII:2021rkn,BESIII:2020uqk])

Our approach can easily provide such an enhancement as seen in the previous figure.

- $1/|\mathcal{J}|_{p\to 0} \to 1/\cos^2\left(\sqrt{2\mu V_a}a\right)$ for an attractive squared-well potential.
- With suitable V_a and a, $1/|\mathcal{J}|_{p\to 0}$ can lead to very large enhancement.

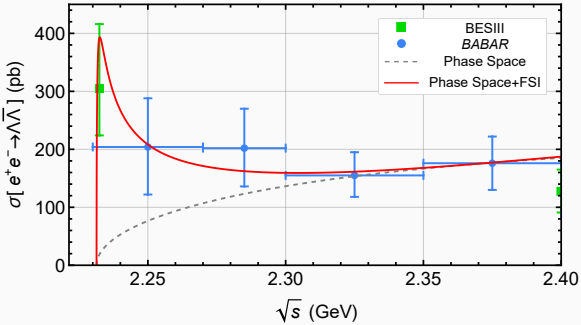
BESIII
BABAR
Phase Space
Phase Space+FSI
σ[e+e−→ΛΛ̄] (pb)
√s (GeV)

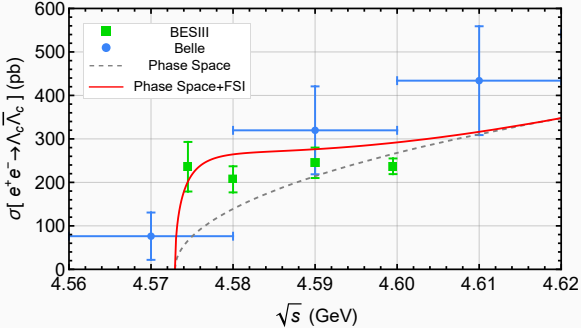
BESIII
Belle
Phase Space
Phase Space+FSI
σ[e+e−→ΛcΛ̄c] (pb)
√s (GeV)

Summary

Summary

In this report, I have briefly discussed possible explanations for the oscillation in the nucleon form factors

- vector meson dominance
- cusp effects from baryon-antibaryon channels
- finite-state interaction effect
- ...

Thank you for your attention!